ORIGINAL ARTICLE

CrossMark

Flow and air conditioning simulations of computer turbinectomized nose models

J. Pérez-Mota[1] · F. Solorio-Ordaz[1] · J. Cervantes-de Gortari[1]

Abstract

Air conditioning for the human respiratory system is the most important function of the nose. When obstruction occurs in the nasal airway, turbinectomy is used to correct such pathology. However, mucosal atrophy may occur sometime after this surgery when it is overdone. There is not enough information about long-term recovery of nasal air conditioning performance after partial or total surgery. The purpose of this research was to assess if, based on the flow and temperature/humidity characteristics of the air intake to the choana, partial resection of turbinates is better than total resection. A normal nasal cavity geometry was digitized from tomographic scans and a model was printed in 3D. Dynamic (sinusoidal) laboratory tests and computer simulations of airflow were conducted with full agreement between numerical and experimental results. Computational adaptations were subsequently performed to represent six turbinectomy variations and a swollen nasal cavity case. Streamlines along the nasal cavity and temperature and humidity distributions at the choana indicated that the middle turbinate partial resection is the best alternative. These findings may facilitate the diagnosis of nasal obstruction and can be useful both to plan a turbinectomy and to reduce postoperative discomfort.

Keywords Unsteady nasal airflow · Computer partial turbinectomy · Nasal surgery simulation

1 Introduction

Air conditioning of the human respiratory system takes place at the nasal cavity. It consists in cleaning, warming, and humidifying the airflow through the small conducts formed in the nose, where the turbinates act as heating and moistening fins for the air intake. Doorly et al. [1] presented an excellent review of the various experimental and numerical methods for modeling airflow in the human nose. The nature and quality of experimental data obtained via model studies were considered, and the potential of newer techniques to improve specific aspects of modeling was discussed. They clearly established that modeling introduces simplifications that may lead to uncertainties or inaccuracies in real life. Both physiologists and modelers need to be fully aware of the shortcomings of modeling in order to make proper interpretations of the information obtained in such studies. There are also a number of related investigations that can be found in the open literature [2–7] where detailed or specific descriptions of the anatomy, physiology, and functions of the human nasal airways are presented, depending on the emphasis and orientation of each investigation.

Any blockage due to malformation or swelling of the nasal conduits generally means the use of the mouth as an alternative air passage. This can lead to harming consequences in the pharynx and related organs and certainly affect the air conditioning functions of the respiratory system. To deal with those obstructions, total or partial resection of turbinates is employed. However, according to the medical practice, the full resection of the turbinates has long-term impairing consequences for the patient, like scab formation, mucosal atrophy, hyperventilation, and nasal dryness, as indicated by Rice et al. [8]. In this respect, Houser [9] pointed out that turbinal tissue is unique and there are no sources in the human body where similar tissue can be extracted to restore a turbinate. Therefore, it is necessary to economize the resecting tissue from a nasal cavity. Indeed, one of the objectives in nasal respiratory investigations is to help the practice of medicine to reduce postoperative discomfort after a nose has been turbinectomized.

✉ J. Pérez-Mota
mota_696@hotmail.com

[1] Departamento de Termofluidos, DIMEI, Facultad de Ingeniería, UNAM Ciudad Universitaria, C.P. 04510 Mexico City, D.F., Mexico

To get a full understanding of the airflow behavior and the air conditioning in pathological and healthy nasal cavities, research work has been conducted in an interdisciplinary framework. This includes experimental and analytical approaches from disciplines like physics, anatomy, physiology, and engineering. They are essential to evaluate the performance of nasal cavities that have experienced some kind of turbinate surgery.

Modeling studies for nasal airflow can be classified in two generic groups: physical models (including body-size scale) and computational representations. Among the first it is worth mentioning for their innovative approach the measurements by Hahn et al. [10] of fluid velocities using hot-wire anemometry in a ×20 enlarged scale model of a healthy nose. They found that in normal respiration there is laminar flow along most of the nasal length. This was also confirmed by Kelly et al. [3], Kim and Son [11], and Hörschler et al. [12] using PIV techniques in laboratory models for similar flow rates during inhalation. The latter authors conducted careful experiments on different transparent models of the nasal cavity, with and without turbinates and spurs. They also included advanced numerical flow simulations and found the significance of geometric changes in the lower turbinate. Important accomplishments on pathological airways models were published by Kim and Chung [13]. They measured airflows in abnormal nasal cavities with PIV methods and surgically created models for the diagnosis of nasal diseases.

On the other hand, mathematical models and the use of computational fluid dynamics (CFD) to obtain a detailed flow structure of the nasal flow have also been successfully used in respiratory fluid dynamics. The contributions of Hörschler et al. [12] and Garcia et al. [14], and the more recent reviews by Leong et al. [15], Zubair et al. [16] and Kim et al. [17] are of note. In them, relevant contributions have been presented to improve and amplify the detailed and general mathematical representation and modeling of nasal airflow. This kind of modeling is part of activity nowadays in the science of CFD, where various flow applications and situations are being modeling together with highly developed computational software. In spite of that, there are still many aspects that need further advance.

To get a full insight into the computer simulation of a turbinectomy and the possible benefit or weakness of a surgery, the operation can be virtually performed by numerical resection of the boundary geometry in the computer model. The results can be compared with those pertaining to the normal case, with special attention to the recirculation zones and swirls produced after turbinectomy.

There are very few numerical investigations in which heat and moisture transfer is considered. In them, a constant temperature is assumed for the boundary representing the nasal mucosa, a situation far from reality as suggested by the results of Lindemann et al. [18, 19].

In fact, Na et al. [20] proposed a variable temperature for the mucosal surface along the conduct, an aspect never examined before. They considered only a steady-state flow, though.

In the present investigation, air conditioning (air warming and humidifying in the nasal cavity) after total and partial resections is considered. A computational and experimental study of the flow and air conditioning in a model of a turbinectomized nose was conducted. This paper presents experimental and computational results aimed to contribute to current physiological research and the practice of medicine related to the health of the respiratory system. This model was conceived and constructed in two steps.

In the first place, X-ray tomographic data were obtained from an in vivo human individual with normal (healthy) nasal cavity. These data served to design and fabricate a 3D printed model of the nose. This model was used as the basic laboratory simulation device (fully described in Section 2.1 below) to measure pressure drop vs. flow rate performance as in a real nasal cavity, and to make verifications of the numerical investigation.

Secondly, numerical (CFD) simulations were performed for seven different cases: a normal nasal cavity and six cases of surgery. Such surgical cases were total resection of the middle turbinate, total resection of the lower turbinate, total resection of both turbinates (middle and lower), partial resection of the middle turbinate, partial resection of the lower turbinate, and partial resection of both turbinates (middle and lower). With these computer numerical models and their appropriate boundary conditions, the flow, energy, and humidity conservation equations were solved to obtain time-dependent (periodic) air conditioned simulations of the cases herein considered, as detailed in Section 2.2.

The purpose of this research was to assess if partial resection is better than total removal of the turbinates based on flow and air conditioning characteristics. For this purpose, numerical simulations of the flow and air conditioning were performed considering time-dependent laminar flow and an extended computational domain. In order to have a complete model, the temperature variation along the mucosal surface and the temperature-dependent diffusivity of water vapor in air were considered. In this research, air conditioning as well as total and partial resection were considered.

In previous investigations, only the airflow changes due to the total resection of the middle and lower turbinates were considered. The possibility of partial resection (as described in the results of this paper) and the air warming and moisturizing of the nasal periodic airflow have not been studied before. The main contribution of the present research is the outline of a method to determine which turbinectomy options could diminish post-surgery symptoms.

2 Methods

2.1 Experimental facility, three-dimensional design, and printing of nasal cavity models

A tomographic study of the nasopharyngeal region of a healthy 21-year-old woman was performed. This study consisted of 171 frontal CT scans (1 mm in-between), each image of 512 × 512 pixels and 0.5 mm/pixel. The images were processed to convert each one into a binary contour adapted to suit the airway. These profiles served to get the X and Y coordinates of each pixel. Fig. 1a shows an example of the CT scans for the normal case, and Fig. 1b–g displays some profiles that conform the shape of the partial and total turbinate resections.

Continuous lines were best-fit to these data using spline functions. With these profile surfaces, the walls of the nasal cavity were drawn, and a volume was produced. The negative

of that volume (Fig. 2a) was printed out using a Connex500 type printer, with FullCure 720 photopolymer material and a precision of 0.2 mm.

The inhalation and exhalation of air from the lungs was assumed to follow a sinusoidal pattern. In order to reproduce the respiratory cycle, an experimental facility was designed and constructed as outlined in Fig. 2b, c. It included a pumping system, two pressure transducers to measure the pressure and flow rate, and a computer to control reproducibility and data acquisition.

The pumping system of the experimental facility consisted of a stepper motor with a maximal angular velocity of 2.5 rev/s, a gear train with a speed ratio of 1:6.25, a ballscrew with a lead of 0.5 cm/rev, a piston-cylinder system (with internal diameter of 15 cm), and a nozzle.

The control of the servomotor and the data acquisition system was performed by the LabVIEW program. It consisted of: a data acquisition system (type PXI-I01I), a universal interface

Fig 1 Outlines of different nasal cavity surgery cases. **a** Example of turbinate scan for the healthy case. Profiles of turbinates for the healthy case at various Z positions. **b** Middle turbinate total resection (MTTR). **c** Middle turbinate partial resection (MTPR). **d** Lower turbinate total resection (LTTR). **e** Lower turbinate partial resection (LTPR). **f** Both turbinates total resection (BTTR). **g** Both turbinates partial resection (BTPR)
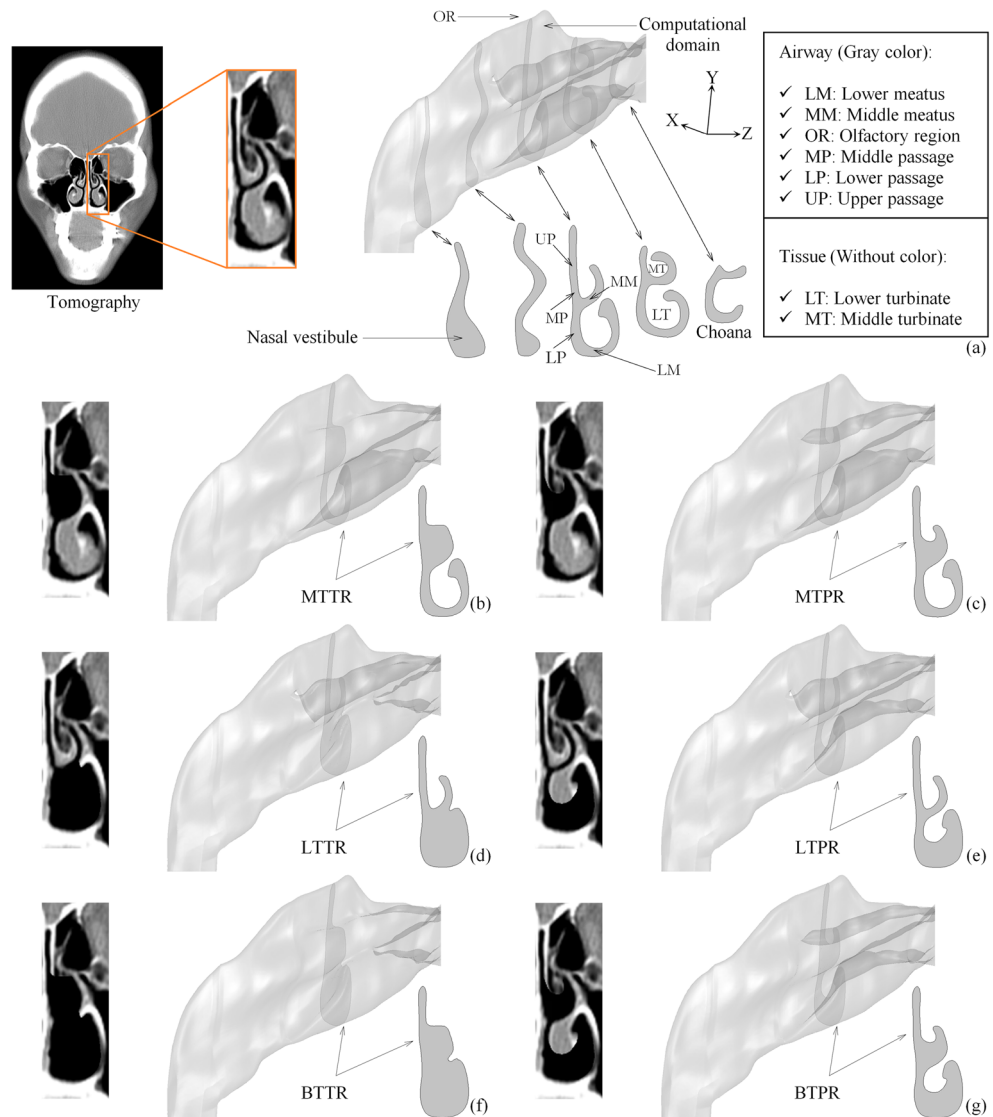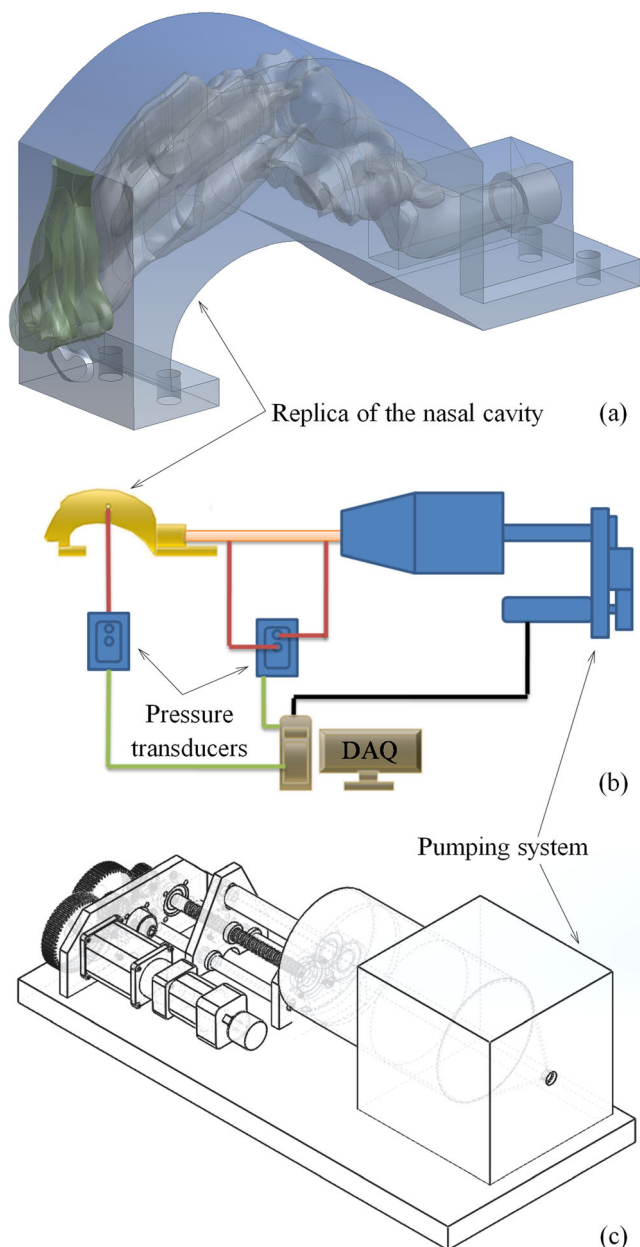
Fig. 2 **a** 3D printed model of the nasal cavity. **b** Experimental facility. **c** Pumping system

for motion (type UMI-7772), a driver system (type BEI5A8), and a power source (type PS16L80). Two differential pressure transducers (type SETRA 264) with a pressure range of − 62.3 to 62.3 Pa and a precision of ± 0.25 were used to measure the pressure drop along the nasal channel.

In the model of the nasal cavity, pressure measurements were performed in the choana. Simultaneously, a second differential pressure transducer was used to measure the mass flow according to Poiseuille equation:

$$\dot{m}_e = \frac{\pi \rho A_{pipe}^2}{8\mu} \frac{dp_{pipe}}{dz} \cong \frac{\pi \rho A_{pipe}^2}{8\mu} \frac{\Delta p_{pipe}}{\Delta z} \tag{1}$$

Laminar regime of the flow was assumed after checking an average Reynolds number of 500 based on the mean fluid velocity and the maximal hydraulic diameter of the normal nasal conduct. The measured pressure vs. flow rate data obtained from the nose model also confirmed this regime. A value of 1.24 was obtained from the data regression for the b exponent in Eq. 2.

$$\Delta p = aQ^b \tag{2}$$

which is in the range generally accepted for laminar flow in this kind of experiments (White [21]).

2.2 Governing equation and computer simulation

2.2.1 Governing equations

The interaction between the airflow and the mucosal lining of a healthy nasal cavity makes possible satisfactory air warming and humidification. To describe this process and detect the changes caused by nasal obstruction or by turbinectomies, the time-dependent equations of mass, momentum, energy, and chemical species conservation (water vapor diffusion from the nasal mucosa into the airflow) were solved for the flow through the nose model. These equations for a general unsteady, laminar, and incompressible fluid motion read (White [21]) as:

Continuity:

$$\nabla \cdot \boldsymbol{U} = 0 \tag{3}$$

Momentum balance:

$$\frac{\partial \boldsymbol{U}}{\partial t} + (\boldsymbol{U} \cdot \nabla)\boldsymbol{U} = -\frac{1}{\rho} \nabla p + \nu \nabla^2 \boldsymbol{U} \tag{4}$$

Energy conservation:

$$\frac{\partial T}{\partial t} + (\boldsymbol{U} \cdot \nabla)T = \frac{k}{\rho c_p} \nabla^2 T \tag{5}$$

Chemical species conservation:

$$\frac{\partial c_{H_2O}}{\partial t} + (\boldsymbol{U} \cdot \nabla)c_{H_2O} = D\nabla^2 c_{H_2O} \tag{6}$$

The computational domain defined for the nasal model (Fig. 3a) was extended downstream and upstream of the nasal cavity numerical domain by coupling a straight duct before the nostril and after the nasopharynx, respectively. The flow was assumed as incompressible, but density and water vapor diffusivity were considered as functions of temperature in the balance equations, respectively, in order to preserve the high sensitivity of these properties to small temperature changes in the mucosal surface.
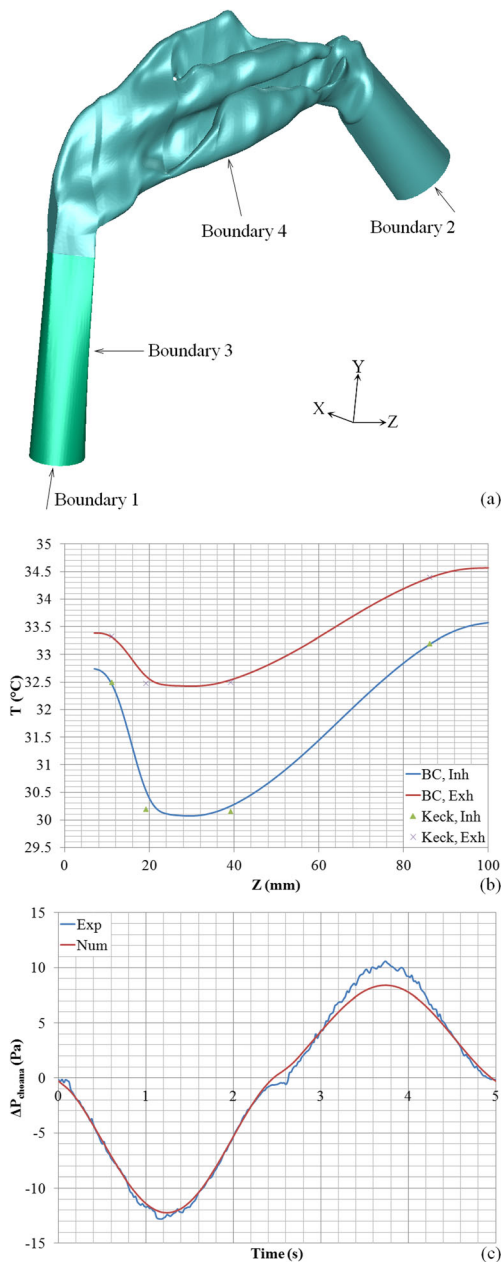
Fig. 3 **a** Computational domain with boundary conditions. **b** Mucosal temperature fitted from the measurements of Lindemann et al. [18]. Blue line represents the temperature boundary condition for $t = 1.25$ s (the maximum velocity is reached at inhalation) and red line represents the temperature boundary condition for $t = 3.75$ s (the maximum velocity is reached at exhalation). **c** Pressure difference along the cavity (present investigation)

A temperature distribution along the wall representing the mucosal surface was established, based on the local temperature measurements by Lindemann et al. [18]. This longitudinal distribution of temperatures was assumed as the average temperature boundary condition for the perimeter of each transverse section of the nasal conduct. A best-fit ninth degree polynomial was proposed for the Lindeman temperature

measurements. Time-dependence of the temperature was considered in the computation process.

2.2.2 Boundary conditions

Some authors include artificial extensions of the nasal cavity for numerical analysis purposes. In general, extending the computational field on both ends of the nasal cavity model (boundary conditions 2 and 3 at the choana and nostril, respectively, in Fig. 3a), allows the flow to get fully developed characteristics avoiding any prevailing or induced flow direction at the ends of the nasal cavity. In any case, to get reliable results and useful designs, the numerical analysis during inhalation must be spread out beyond the numerical computing mesh. This is to get appropriate mathematical boundary conditions at the entrance and at the exit of the nasal cavity model. Otherwise, there is a risk of imposing a boundary condition that does not properly fit into the physical reality of the nasal cavity being modeled. This implies that the numerical mesh includes the pharynx. Some authors have modeled the remainder of the pharynx as a cylindrical extension duct. Boundary conditions for the inhalation and the exhalation phases of the respiratory cycle were assumed as follows:

Inhalation A mass flow rate given by Eq. 7 normal to boundary 1 was specified (Fig. 3a), and a water vapor mass fraction of 5.12×10^{-3} kg H_2O/kg humid air was set. This corresponds to a relative humidity of 30% with a temperature of 18 °C and a pressure of 76.9 kPa. At boundary 2, longitudinal gradients of velocity, temperature, and humidity were assumed null.

$$\dot{m} = \frac{\pi}{16} L D_P^2 \rho \omega_r \sin(\omega_r t) \qquad (7)$$

Exhalation At boundary 1, the longitudinal gradients of velocity, temperature, and humidity were assumed zero. A mass flow given by the negative of Eq. 7 and perpendicular to boundary 2 was specified (Fig. 3a); on this boundary, a temperature of 36.5 °C and a variable mass fraction (Eq. 8) were assumed to get a relative humidity close to 100%. The average pressure in boundary 2 was obtained from a previous cycle, when only the mass and momentum equations were solved.

Inhalation and exhalation At boundary 3 (Fig. 3a), a water vapor mass fraction equal to 5.12×10^{-3} kg H_2O/kg humid air was set, which corresponds to a relative humidity of 30%, a temperature of 18 °C, and a pressure of 76.9 kPa. Boundary 4 represents the nasal mucosa. No slip condition was assumed at the boundary 4 and the temperature-time variable was assigned through ninth degree polynomials which were variables with the position on the Z axis. These functions were obtained from measurements of temperature in the nasal mucosa made by Lindemann et al. [18] on 15 volunteers.

Figure 3b shows the temperature in the mucosal surface at 1.25 and 3.75 s, respectively, where the functions defined by the polynomials attain their minimum and maximum values, respectively. Relative humidity at boundary 4 was 100% and the water vapor mass fraction was set through Eq. 8.

$$MF_{vapor} = \cfrac{1}{1 + \cfrac{1}{0.622 \left[\cfrac{\phi p_{sat}}{p - p_{sat}} \right]}} \tag{8}$$

2.3 Solution method

Equations 3 to 6 with boundary conditions 7 and 8 were solved using a commercial finite volume package. An atmospheric pressure of 76.9 kPa was set. Furthermore, the following air thermophysical properties were considered: $\mu = 1.82 \times 10^{-5}$ kg m^{-1} s^{-1}, $k = 0.025$ Wm^{-1} K^{-1}, and $C_P = 1007$ J kg^{-1} K^{-1}, and density and mass diffusivity of water vapor in air were taken as temperature-dependent according to Eqs. 9 and 10.

$$\rho = \left(2.29 - 10.83 \times 10^{-3} T + 13.08 \times 10^{-6} T^2 \right) \left[\text{kg/m}^3 \right] \tag{9}$$

$$D = \left(1.538 \times 10^{-9} T^{1.75} \right) \left[\text{m}^2/\text{s} \right] \tag{10}$$

The first-order upwind scheme was employed for discretization of the previous equations. A segregated solver with the SIMPLE scheme ([22]) was used for coupling pressure and velocity. The convergence criterion for the residuals of continuity and velocity components were 1×10^{-5}, for energy and chemical species conservation were 1×10^{-7}. All the geometries studied were meshed using the Cut Cell Method of ANSYS, and a time step size of 0.05 s was used.

In order to validate the numerical model, a respiratory frequency of 12 cycles/min with a tidal volume of 0.5 l was employed. Numerical and experimental pressure data were compared at the choana (Fig. 3c).

3 Results

The raw data obtained from the solution of equations and computer simulations consist of 3D velocity vectors, temperature, and water vapor distributions in the nose flow fields for every simulated case, as shown in Figs. 4, 5 and 6. The data compose a complex and full set of numerical results representing the variables and functions of the model. In order to make full use of them and get practical graphical descriptions of the various flow cases, descriptive diagrams, cross sections, and flow lines were established. Temperature and concentration isosurfaces were also computed to better illustrate the flow behavior. Cross sections to the Z axis were

defined at intervals of 1 mm. Velocity vectors and streamlines were carefully reviewed for each cross section in order to detect any recirculation and/or swirls zones. In the paragraphs that follow, a full description of the graphical representation of the simulation for the six cases is presented.

3.1 Normal nasal cavity and effects of a spur

There is a recirculation zone approximately 12 mm in length, located in the nasal vestibule for the healthy nasal cavity: flow pattern tagged as A in Fig. 4. Structure A is revealed in the same location for all cases. Starting at $Z = 18$ mm, this flow structure emerges from the sudden contraction of the nasal vestibule, right before the beginning of the turbinates. This recirculating air is in contact with the mucosal surface for a longer time, giving rise to more heat and humidity transfer to the air, as can be seen in the temperature profiles for $Z = 26$ mm in Fig. 4. In all the regions where these structures were identified, the temperature and humidity are higher than in the neighboring streamlined regions, as seen in the temperature and humidity profiles of Figs. 4, 5 and 6

A second recirculation zone of 9 mm in length was detected at the medial passage of the nasal cavity at one side of the middle turbinate, B pattern at $Z = 42$ mm in Fig. 4. It is originated by a small spur located 10 mm upstream. As seen at $Z = 50$ mm, temperature and humidity are smaller in the lower passage than in the middle of the conduit.

In the olfactory region, on the other hand, there is a low-velocity zone corresponding to the flow direction changes due to the sphenoidal sinus (pattern C in Fig. 4). The temperature and humidity are higher than in the neighboring zones of the upper passage, as seen in the profiles of Fig. 4.

3.2 Middle turbinate: comparison of total against partial resection

Two eddies emerge in the case of total resection of the middle turbinate, D and E structures, respectively in Fig. 5a. They are directly associated to an abrupt expansion due to the removal of the spur and to the space left by the resected middle turbinate. Both eddies arise at $Z = 42$ mm: the first one of approximately 29 mm length and the second one of about 35 mm.

In the partial resection of the middle turbinate, there is one eddy very similar to structure D, referred here as the D′ structure (Fig. 5b). The location of the D′ structure occurred at the same place because it was produced by the removal of the spur. The most evident characteristic of this structure, as compared to the total resection of the middle turbinate, is its length of 22 mm (7 mm smaller than the D structure) and its helical shape. This means that the flow is more stable and persistent. This is so because a smaller amount of turbinate was removed.

The air trapped within eddies is warmer and more moist than the air left outside the vortices. To evaluate the
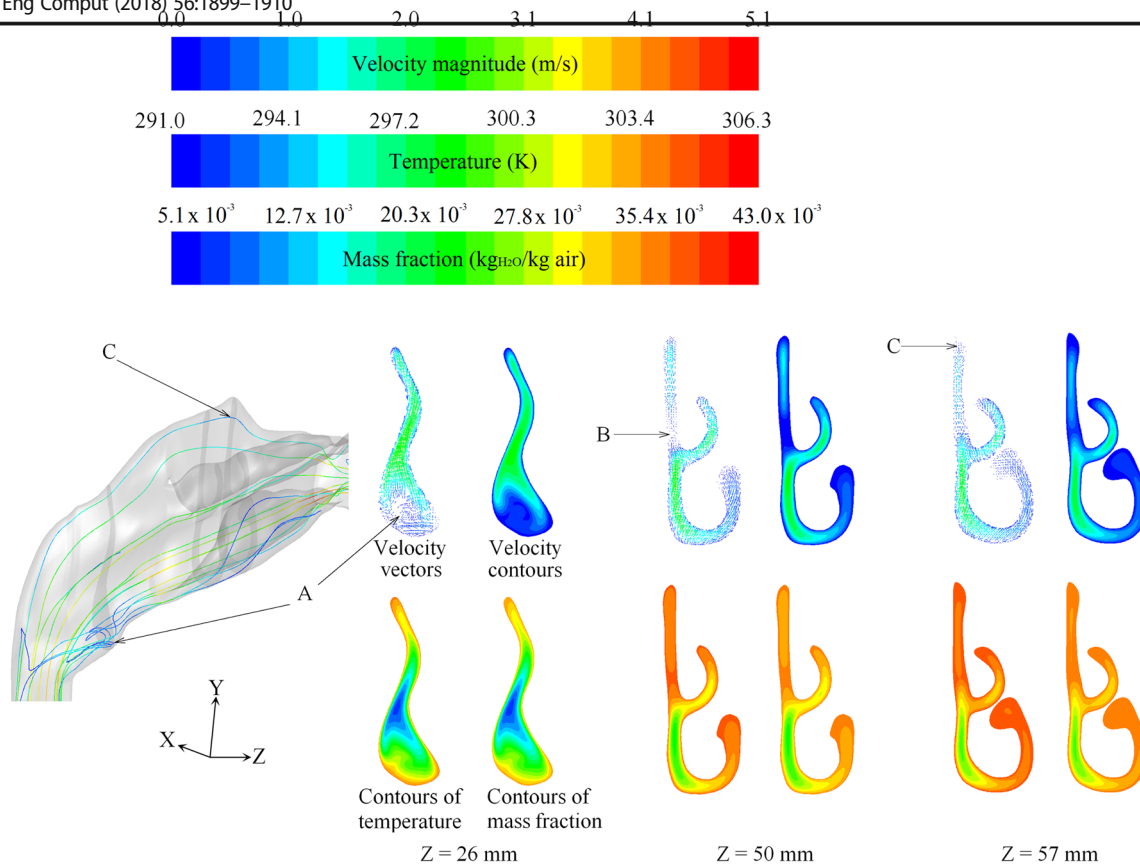
Fig. 4 Typical 3D velocity vector profiles, temperature, and water vapor distributions in the nasal flow fields from the solution of equations and computer simulations. Normal (healthy) case

effectiveness of the air conditioning of temperature, isothermal surfaces were computed and graphically presented in Fig. 6. A seen in Fig. 6b, c, the isothermal surface corresponding to the partial resection of the middle turbinate is shorter than the one obtained for the total resection of the middle turbinate. This implies that for the partial resection of the middle turbinate, the air reaches a temperature above 300 K after 61 mm. For the case of total resection of the middle turbinate, it occurs after 65 mm. For the results, presented air conditioning is better with partial resection rather than total resection of the middle turbinate.

3.3 Lower turbinate: total vs. partial resection

When the lower turbinate is completely removed, a vortex 37 mm in length is formed at $Z = 40$ mm (F pattern, Fig. 5c). This flow pattern is chaotic and fills most of the space left by the lower turbinate. This fluid response indicates that total resection of the lower turbinate was excessive. When the lower turbinate is partially removed, a vortex 35 mm in length is developed at the inferior meatus (F′ pattern in Fig. 5d).

Regarding the size of the isothermal surfaces, they are longer in the case of partial resection as compared to the total resection of the lower turbinate, as can be seen in Fig. 6d, e. It means that thermal conditioning is slightly better in the second

case. It can also be noted that both resection cases resemble the healthy one. This fact can be misinterpreted if the remarkable changes in the flow structure and the amount of removed tissue were not taken into account as discussed in a following section.

3.4 Both turbinates: comparison of total against partial resection

Three eddies emerge for the extreme case where both the middle and lower turbinates are removed. Two of them are similar to D and E flow structures because they have almost the same characteristics of length and location. The third one is like the F pattern, except in the direction of the flow at the end of the vortex that changed slightly (Fig. 5e). Only two eddies emerge in the case where the middle and lower turbinates are partially removed; they have the same characteristics as the D′ and F′ patterns in terms of length and shape (Fig. 5f).

The cross-sectional area substantially increased for the cases of resection of both turbinates. As a direct consequence of this, the pressure increased in the region between $Z = 40$ mm and $Z = 80$ mm. This effect is stronger in the case of total resection than in the case of partial resection and can be verified with Bernoulli's equation.
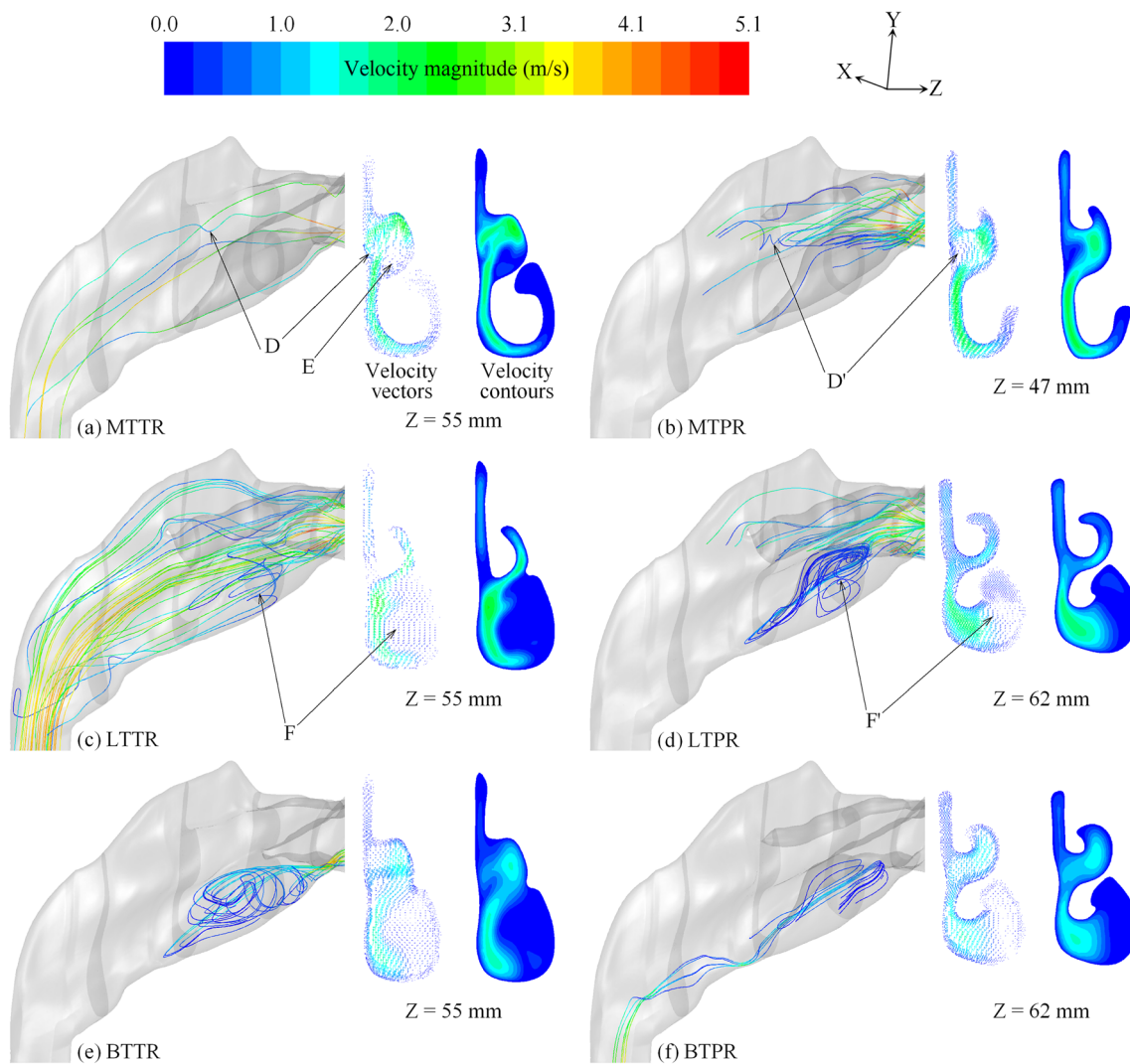
Fig. 5 Pathlines, and at different cross sections, velocity vectors and velocity contours colored by velocity magnitude corresponding to the maximal flow rate during inhalation: (a) Middle turbinate total resection (MTTR), (b) Middle turbinate partial resection (MTPR), (c) Lower turbinate total resection (LTTR), (d) Lower turbinate partial resection (LTPR), (e) Both turbinates total resection (BTTR), (f) Both turbinates partial resection (BTPR)

The isothermal surfaces in Fig. 6f, g indicate that the conditioning is better in the partial resection than in the total resection of both turbinates. Temperature distributions appear to be a combined effect of the two behaviors described in the previous sections.

4 Discussion

A detailed analysis of a healthy nasal cavity geometry shows that the turbinates form a set of narrow channels for streamlined airflows. The anatomical diversity of the nasal cavity and the way that a nasal obstruction can affect the patient give rise to a large number of possible geometries and consequent flow patterns. To emulate these flows and achieve general results, it was considered

that the nasal cavity reduces completely the swelling after the turbinectomy. This assumption can be used for assessment of surgery through computer simulations as a supplementary exploration to respiratory monitoring in medical care (Folke et al. [23]).

Six cases of computer turbinectomized nasal cavities were compared with a normal, non-surgery one. The results were presented using typical flow characteristics: streamlines, velocity, temperature and humidity distributions, and the extent of isothermal surfaces within the cavity. The turbinectomies correspond to partial or total removal of the middle and lower turbinates, respectively. It was observed that the flow is strongly distorted due to the turbinal tissue removal as recirculation zones were clearly visible. In fact, for the case of total resection of the middle turbinate, eddies may form between the main

Fig. 6 Isothermal surfaces corresponding to the maximal flow rate during inhalation. **a** Healthy case. **b** Middle turbinate total resection (MTTR). **c** Middle turbinate partial resection (MTPR). **d** Lower turbinate total resection (LTTR). **e** Lower turbinate partial resection (LTPR). **f** Both turbinates total resection (BTTR). **g** Both turbinates partial resection (BTPR
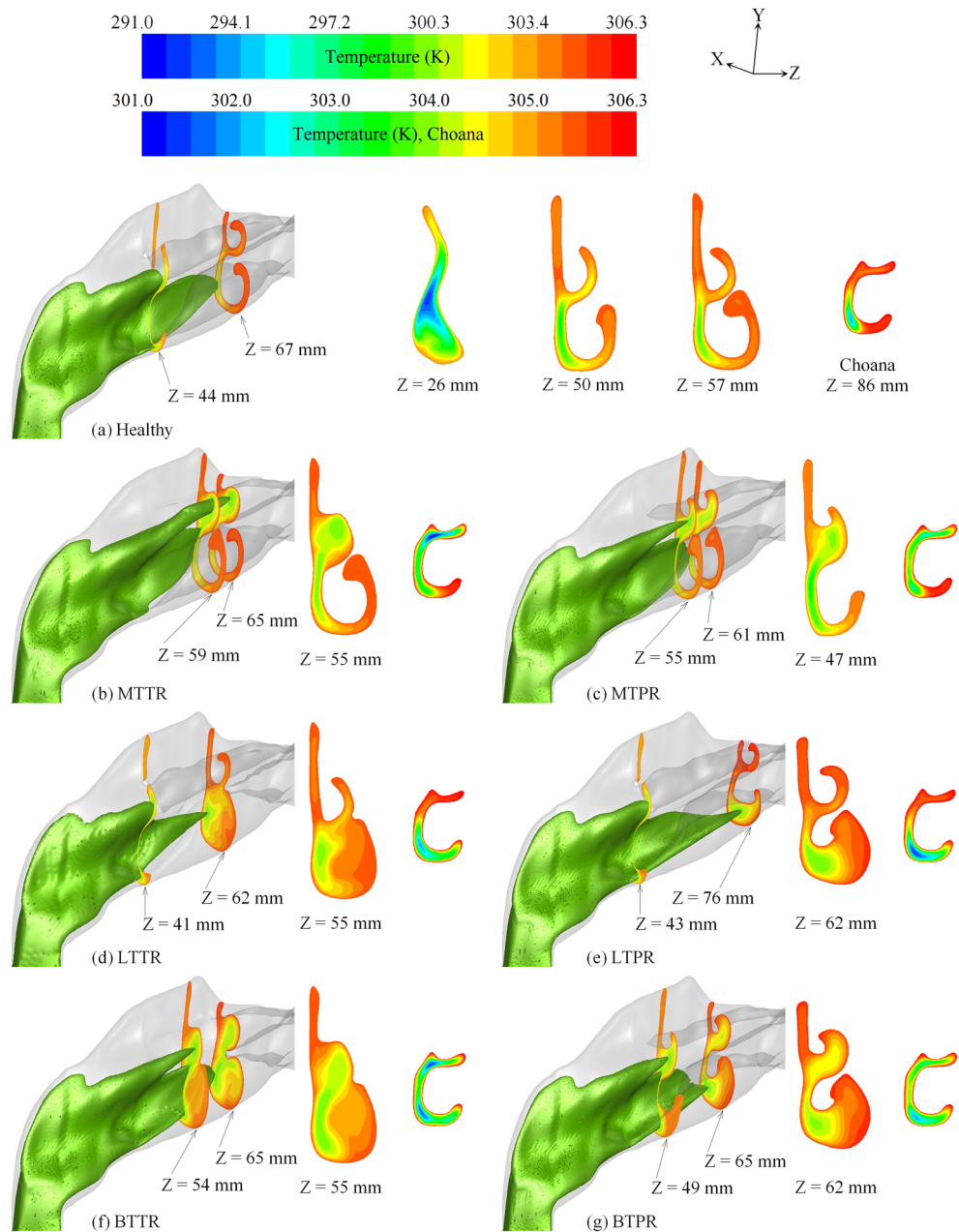
airflow and the mucosal surface preventing their full interaction and the proper air conditioning.

Higher than normal temperature and humidity values were observed with these flow structures. This is due to more time being spent by air in contact with the nasal mucosa in these recirculation zones. On the contrary, as the flow resistance decreases when the middle turbinate is fully or partially removed, the mainstream velocity increases and the air warms up a little bit. This is confirmed by the extent of the isothermal surfaces since these are longer when middle turbinate resection is performed as compared with the non-surgery case. On the other hand, when the lower turbinate is fully or partially removed,

eddies resulted in a flow resistance increase. Therefore, the mainstream velocity is almost the same as in the non-surgery case leading to isothermal surfaces almost the same size as in the non-resected case.

Table 1 shows the pressure difference between the nostril and the choana, Δp, for the cases herein reported. If the pressure drop is taken as the only criterion to practice a turbinectomy, it would seem that the best option would be to partially remove the lower turbinate. This is so since the pressure drop after this resection is close to the non-surgical case. Nevertheless, if the flow patterns in all cases of surgery are reviewed looking at the recirculation and eddies formation, the cases that involve the lower

Table 1 Pressure difference between the nostril and the choana (Pa), percent of mesh elements at the choana with temperature smaller than 304.6 K, temperature at the choana (K), and mass fraction MF (1×10^{-3} kg H$_2$O/kg humid air)

Case	Δp (Pa)	Percent of elements with $T > 304.6$ K	T (K)	MF 1×10^{-3} (kg$_{water}$/kg$_{humid\ air}$)
Total resection of both turbinates	− 9.7	56.9	304.2	37.2
Total resection of the middle turbinate	− 8.4	68.4	304.7	38.1
Partial resection of both turbinates	− 10.1	66.9	604.6	37.9
Partial resection of the middle turbinate	− 10.7	75.4	305.0	39.4
Total resection of the lower turbinate	− 8.3	30.2	304.58	37.93
Partial resection of the lower turbinate	− 10.9	76.1	304.8	28.3
Healthy	− 12.3	88.7	305.3	39.4

turbinate resection could be discarded instead, concluding then that partial or total resection of the middle turbinate might be taken as the best alternatives.

Temperature or mass fraction of water vapor distributions in the choana can be used to select one of the two remaining cases: either the total or the partial resection of the middle turbinate. Figure 6 shows the temperature distribution for all the geometries studied. As seen, the temperature distributions corresponding to the partial resection of the middle turbinate are more similar to the non-surgery case than the total resection of the middle turbinate. This is confirmed by the large quantity of mesh elements at the choana that attain temperatures higher than 304 K as shown in Table 1. The average mass fraction in Table 1 also indicates that the partial resection of middle turbinate is very much like the normal case. In summary, the streamlines and the temperature and humidity distributions in the choana indicate that the middle turbinate partial resection is the best alternative.

Earlier investigations by other authors addressed a variety of turbinectomy practices that are somewhat different but complementary to the ones reported in this paper. For instance, Chung and Kim [24] studied unsteady flow in a nasal cavity model using PIV techniques for some turbinectomy variations for the middle and lower turbinate; the results reported in the present research compare well with those reported by these authors. Hörschler et al. [12] performed similar simulations in the steady-state including a case with spurs. In both investigations, the air conditioning of the nose cavity was not included. Na et al. [20] studied some lower turbinate surgeries but their research was conducted in the steady-state.

In fact, all the abovementioned authors did not consider the following surgeries: partial resection of the middle turbinate and partial resection of the middle and lower turbinate, reported as cases (c) and (g) respectively in the present investigation, as shown in Fig. 1. According to the results of this research, the middle turbinate partial resection is one of the surgeries with greatest potential for reducing postoperative discomfort.

The results reported by Chung and Kim [24] during inhalation showed that the main flow path occurred through the middle passage, whereas in the present work, it was through the lower passage; the flow preference for either one of the two passages, middle or lower, can be attributed to two important anatomical aspects: the first one is that the middle passage is slightly wider than the lower passage in the geometry of Chung and Kim; the second one is that in our geometry there is a spur in the middle passage.

For a patient with atrophic rhinitis in the inferior portion, i.e., at the region where the lower turbinate should be, a low-velocity eddy was observed by Garcia et al. [14]. For the case of the lower turbinate total resection, Chung and Kim [24] show the distribution of RMS velocities in some coronal planes; in their results, there is a maximum of RMS velocity in the airway enlarged by the removal of the lower turbinate; this is an indication of the presence of vortical structures. Furthermore, for the lower turbinate resection, Na et al. [20] pointed out the formation of a spiral type vortical structure. All the authors referred to in this paragraph found the presence of a vortex in the space left by the lower turbinate resection; this fact is consistent with the results of this work.

On the other hand, temperature measurements at the nasopharynx have been previously reported only by Lindemann et al. [19]. They reported a temperature of 32.5 °C, meaning 7.5 °C above the room temperature of 25 °C during their experiments. This temperature is reached during the inhalation phase when the maximum velocity occurs in this stage of the respiratory cycle. In the present work, at the nasopharynx in $Z = 91$ mm the average temperature was 25.5 °C, which means that the temperature increase was also 7.5 °C. There are no reports in the open literature on the mucosal temperature and the airway temperature for the same patient; therefore, in the present investigation, the temperature boundary condition at the mucosal surface is based only on the temperature measurements made by Lindemann et al. [18].

Finally, regarding the unsteady-state flow pattern in the nasal cavity, the findings by Lee et al. [25] reported that the exhalation stage lasts longer than the inhalation

phase. This points out a limitation of our simulations because an exact sinusoidal function was set as boundary condition to represent the whole respiratory cycle. The use of a sinusoidal pattern provides specific results that can be considered for certain flow characteristics related to inertial effects that are not included in the present research, as has been reported by Hörschler et al. [12].

5 Conclusions

After turbinectomy, one symptom that occurs in the long term is the atrophy of the nasal mucosa, augmented by the excessive removal of the turbinal tissue. This is an important reason to plan surgery.

Nasal cavity swelling causes a relatively large pressure drop and removal of the turbinates is an alternative to improve the patient breathing in the short term.

An extensive literature search was conducted resulting in a shortage of experimental data related to the nasal cavity mucosal temperature. Specifically, there are not any in vivo temperature data for the nasal mucosa and the airway of the same patient. This is the reason why a boundary condition based on the temperature measurements of Lindemann et al. [18] was established at the wall representing the mucosal surface, and the mean temperature at the level of nasopharynx was computed and compared with the data of Lindemann et al. [19].

For the six different surgery cases herein reported, the difference of the average temperature at the choana in the worst case with respect to the healthy case is no more than 2 °C. This variation may seem insignificant, but it might be one of the variables that after some years cause mucosal atrophy.

The capacity for heating and humidifying the air is substantially reduced with the total removal of the turbinates, and the flow shows evident recirculation zones and swirls. These features are undesirable because they affect the natural velocity distribution and give rise, as a consequence, to the atrophy of the remaining mucosa.

When the turbinates are partially removed, it was observed that recirculation zones and eddies are not so marked and little turbinal tissue is removed. According to our results in Table 1, partial and total resections of the middle turbinate are good options to correct the nasal obstruction.

Glossary

|	
Δp	Pressure difference between nostril and choana (Pa)
Δp_{pipe}	Pressure drop for Poiseuille flow (Pa)
Δz	Distance between pressure ports for Poiseuille flow (m)
ϕ	Relative humidity
μ	Air dynamic viscosity (kg $m^{-1}s^{-1}$)
ρ	Air density (kg/m³)
ω_r	Respiratory frequency (rad/s)
$\dot{m}$	Boundary condition mass flow rate (kg/s)
$\dot{m}_e$	Experimental mass flow rate (kg/s)
a, b	Empirical constants
c_{H_2O}	Water vapor concentration in air $(kg_{H_2O}/kg_{humid\ air})$
c_p	Air specific heat at constant pressure (J $kg^{-1}K^{-1}$)
A_{pipe}	Cross-sectional area for Poiseuille flow (m²)
D	Diffusivity of water vapor in air (m²/s)
D_P	Piston diameter (m)
k	Air thermal conductivity (W $m^{-1}K^{-1}$)
L	Piston travel length (m)
MF_{vapour}	Water vapor mass fraction $(kg_{H_2O}/kg_{humid\ air})$
p	Pressure (Pa)
p_{sat}	Saturation pressure (Pa)
Q	Volume flow (m³/s)
T	Temperature (K)
t	Time (s)
U	Velocity vector (m/s)
v	Air kinematic viscosity m²/s

References

1. Doorly DJ, Taylor DJ, Schroter RC (2008) Mechanics of airflow in the human nasal airways. Res Phys Neurobiol 163:100–110
2. Mygind N, Dahl R (1998) Anatomy, physiology and function of the nasal cavities in health and disease. Adv Drug Deliv Rev 29(1/2):3–12
3. Kelly JT, Prasad AK, Wexler AS (2000) Detailed flow patterns in the nasal cavity. J Appl Physiol 89:323–337
4. Naftali S, Rosenfeld M, Wolf M, Elad D (2005) The air-conditioning capacity of the human nose. Ann Biomed Eng 33:545–553
5. Kim JK, Yoon JH, Kim CH, Nam TW, Shim DB, Shin HA (2006) Particle image velocimetry measurements for the study of nasal airflow. Acta Otolaryngol 126:282–287
6. Taylor DJ, Doorly DJ, Schroter RC (2010) Inflow boundary profile prescription for numerical simulation of nasal airflow. J R Soc Interface 7:515–527
7. Gambaruto AM, Taylor DJ, Doorly DJ (2012) Decomposition and description of the nasal cavity form. Ann Biomed Eng 40:1142–1159
8. Rice DH, Kern EB, Marple BF, Mabry RL, Friedman WH (2003) The turbinates in nasal and sinus surgery: a consensus statement. Ear Nose Throat J 82:82–84
9. Houser SM (2007) Surgical treatment for empty nose syndrome. Arch Otolaryngol Head Neck Surg 133:858–863
10. Hahn I, Scherer PW, Maxwell M (1993) Mozell velocity profiles measured for airflow through a large-scale model of the human nasal cavity. Appl Phys 75:2273–2287
11. Kim SK, Son YR (2004) Investigation on airflows in abnormal nasal cavity with adenoid vegetation by particle image velocimetry. KSME Int J 18:1799–1808

12. Hörschler I, Brücker C, Schröder W, Meinke M (2006) Investigation of the impact of the geometry on the nose flow. Eur J Mech B Fluids 25:471–490

13. Kim SK, Chung SK (2004) An investigation on airflow in disordered nasal cavity and its corrected models by tomographic PIV. Meas Sci Technol 15:1090–1096

14. Garcia GJM, Bailie N, Martins DA, Kimbell JS (2007) Atrophic rhinitis: a CFD study of air conditioning in the nasal cavity. J Appl Physiol 103:1082–1092

15. Leong SC, Chen XB, Lee HP, Wang DY (2010) A review of the implications of computational fluid dynamic studies on nasal airflow and physiology. Rhinology 48:139–145

16. Zubair M, Abdullah MZ, Ismail R, Shuaib IL, Hamid SA, Ahmad KA (2012) Review: a critical overview of limitations of CFD modeling in nasal airflow. J Med Biol Eng 32:77–84

17. Kim SK, Na Y, Kim JI, Chung SK (2013) Patient specific CFD models of nasal airflow: overview of methods and challenges. J Biomech 46:299–306

18. Lindemann J, Leiacker R, Rettinger G, Keck T (2002) Nasal mucosal temperature during respiration. Clin Otolaryngol 27: 135–139

19. Lindemann J, Kühnemann S, Stehmer V, Leiacker R, Rettinger G, Keck T (2001) Temperature and humidity profile of the anterior nasal airways of patients with nasal septal perforation. Rhinology 39:202–206

20. Na Y, Chung KS, Chung SK, Kim SK (2012) Effects of single-sided inferior turbinectomy on nasal function and airflow characteristics. Respir Physiol Neurobiol 180:289–297

21. White FM (2009) Fluid mechanics, 7th edn. McGraw-Hill, New York

22. FLUENT 6.3 User's Guide, September 2006, Lebanon, NH 03766, USA

23. Folke M, Cernerud L, Ekström M, Hök B (2003) Critical Review of non-invasive respiratory monitoring in medical care. Med Biol Eng Comput 41:377–383

24. Chung SK, Kim SK (2008) Digital particle image velocimetry studies of nasal airflow. Respir Physiol Neurobiol 163:111–120

25. Lee JH, Na Y, Kim SK, Chung SK (2010) Unsteady flow characteristics through a human nasal airway. Respir Physiol Neurobiol 172:136–146

José Eduardo Pérez-Mota
BSME University of Guanajuato, Mexico (UG, 2008). MSME National University of Mexico (UNAM) 2011 with honors. Assistant Professor at UNAM, thermofluids laboratory and fluid mechanics
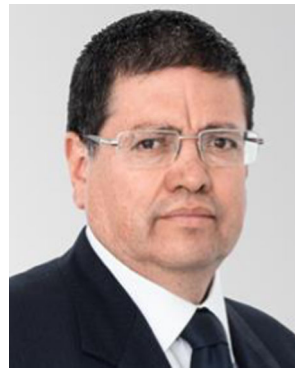
Francisco J. Solorio-Ordaz
Professor of ME, National University of Mexico (UNAM). BSME (UMSNH, 1977), MSME (UNAM, 1981), and PhD (UNAM, 1989). Author and co-author of more than 70 publications. President of the Mexican Society of Mechanical Engineering (1998–2000). Was the Chairman of Thermofluids Department for more than 20 years and currently Head of the Mechanical and Industrial Division at the School of Engineering of UNAM

Jaime Cervantes-de Gortari
Professor of ME, National University of Mexico (UNAM). BSME (UNAM, 1970), MSME (UNAM, 1972), and PhD (Purdue, 1976). Author and co-author of more than 150 publications including textbooks, monographs, and original research papers. Fellow of ASME